Soft X-ray absorption and EXAFS on the K edge of aluminium

1979 J. Phys. F: Met. Phys. 9 2143

(http://iopscience.iop.org/0305-4608/9/10/023)

J. Phys. F: Metal Phys., Vol. 9 No. 10, 1979. Printed in Great Britain

Soft x ray absorption and EXAFS on the K edge of aluminium

A Fontaine†‡, P Lagarde†‡, D Raoux†‡ and J M Esteva§

† LURE, CNRS, Laboratoire associé à l'Université de Paris-Sud, Bâtiment 209 C, 91405 Orsay, France

‡ Laboratoire de Physique des Solides, Université de Paris-Sud, Laboratoire associé au CNRS, Bâtiment 510, 91405 Orsay, France

§ LURE and ERA 719, Laboratoire de Spectroscopie Atomique et Ionique, Université de Paris-Sud, Bâtiment 350, 91405 Orsay, France

Received 14 March 1979, in final form 18 May 1979

Abstract. This paper reports EXAFS (extended x ray absorption fine structure) measurements performed in the 1000–2500 eV range using synchrotron radiation delivered by the ACO storage ring (LURE). The K edge EXAFS spectra of Al in elemental aluminium and α alumina have been analysed: it is shown that accurate measurements of the first-neighbour distances are possible even for low-Z atoms. In the case of the metal, we emphasise the importance of the screening of the core hole potential in the first 150 eV part of the spectrum.

1. Introduction

Extended x ray absorption fine structure (EXAFS) studies in the soft x ray region have suffered up to now from a lack of x ray sources with sufficiently high intensity and also from a lack of efficient monochromators. Synchrotron radiation from storage rings is now available in the whole x ray range, and soft x ray absorption experiments are now feasible on the K edges of light elements. Recently, EXAFS and surface EXAFS between 300 eV and about 1000 eV have been performed (Stöhr *et al* 1978a, Bianconi and Bachrach 1979) using a grating monochromator (Brown *et al* 1978) and electron yield techniques. We report here photo-absorption measurements performed at the ACO storage ring† on the Al K edge (1559·3 eV) in pure aluminium and αAl_2O_3 which are to our knowledge the first EXAFS experiments in the 1 to 2·5 keV range using synchrotron radiation. The monochromator used was a two-crystal Bragg spectrometer designed at LURE (Lemonnier *et al* 1978). Absorption spectra have been recorded over 1000 eV in a few hours. Near the edge, our measurements are in good agreement with the edge structure measurements already performed with conventional x ray tubes on aluminium (Cauchois 1962, Nagakura 1964, Deslattes 1969, Senemaud and Costa Lima 1976); however, the high photon intensity delivered by ACO results in a considerable gain of time, which makes practical EXAFS measurements

† We are grateful to the Laboratoire de l'Accélérateur Linéaire at Orsay for building the ACO storage ring.

0305-4608/79/102143+11 $01.00

over several hundreds of eV. Our experimental set up thus covers the range 20 to 4 Å, which is intermediate between conventional EXAFS measurements ($\lambda < 4$ Å) and soft x rays EXAFS measurements using electron yield spectroscopy ($\lambda > 15$ Å).

Significant EXAFS structures have been found as far as 250 eV above the Al K edge and they have been analysed using the now classical EXAFS theory (Sayers *et al* 1970, Ashley and Doniach 1975). Nearest-neighbour distances have been obtained for both aluminium and α alumina with an accuracy of better than 0·01 Å. This shows that, as noticed by Stöhr (1979), accurate measurements of bonding distances can be obtained even for low-Z atoms where the EXAFS oscillations do not extend far more than 200 or 300 eV above the edge. However, we also show that, in the case of a metal like Al, the screening of the core hole potential cannot be neglected in the analysis of the first 150 eV of EXAFS signal above the edge. This is in agreement with a semiclassical model for the screening of the core hole (Noguera *et al* 1979).

2. Experimental technique

2.1. Experimental set up

The Bragg monochromator is a two-crystal device with parallel mounting. The height of the outgoing beam is kept constant by controlling the distance between the two crystals as they rotate. This is a very convenient and simple arrangement for a high-vacuum instrument (10^{-7} Torr). Technical details concerning the monochromator have already been published (Lemonnier *et al* 1978). A thin beryllium window (12·5 μm) is placed in front of the monochromator to filter the visible and UV light emitted by ACO. The crystals used are organic KAP with a $2d$ spacing of 26·63 Å. They are 1 cm wide, so that about 1 mrad of the emitted beam was used. It has to be pointed out that organic crystals—like KAP—are severely damaged by the very intense photon flux delivered by ACO. Their reflectivity decreases by almost two orders of magnitude in the first few hours of exposure. After this stage, however, it remains constant even after weeks of exposure. No damage has been found with mineral crystals like quartz, mica or beryl; they are however not suitable for EXAFS studies between 600 and 2000 eV since they contain many of the lighter elements.

We used as a detector either an ion chamber or a channel plate. The ion chamber was filled with 300 Torr of argon and had a 3 μm thick Mylar window which does not absorb more than a few per cent of the incident x ray beam in the 1 to 2 keV region. When ACO was operated at 540 MeV and 100 mA, the output current of the ion chamber was typically of the order of 10^{-11} A and the counting rate of the channel plate was of the order of 10^5 counts s^{-1}, as is shown in figure 1. Signal-to-noise ratios were quite similar for both detectors in this energy range. Channel plates are better for photon energies lower than 800–1000 eV. Their efficiency is about 1%. This means that about 10^7 photons s^{-1} eV^{-1} $mrad^{-1}$ are typically transmitted by the monochromator and the 12 μm thick beryllium window. Because of the large critical wavelength of ACO ($\lambda_c = 38$ Å) the photon flux decreases drastically with the photon energy above 2 keV: then, when working in the 1·5–2·5 keV range, almost no second-order beam is transmitted through the monochromator.

The whole experiment is monitored by a Tektronix 4051 computer, which automatically rotates the monochromator and stores the data.

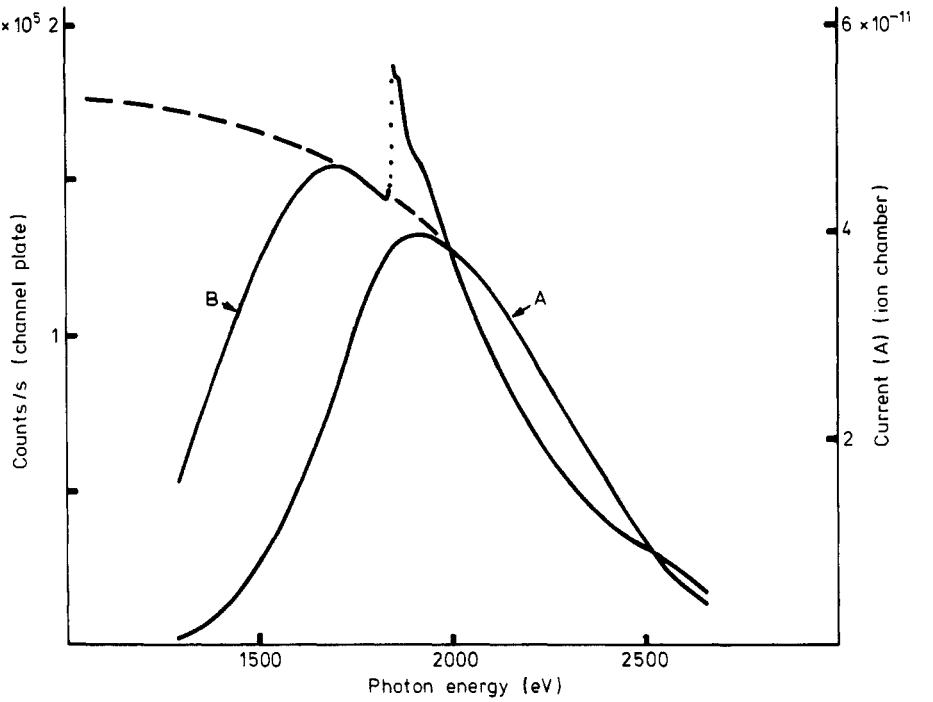

Figure 1. Photon flux emerging from the monochromator measured as the output current of a ion chamber (A) and the counting rate of a channel plate (B). The sharp cut-off at low energies is due to the relative arrangement of the two crystals, which is optimised for photon energies around 2 keV, but is not the best at energies lower than 1·5 keV. The actual ACO photon flux is schematically shown by the broken line. The peak at about 1850 eV found on curve B is due to silicon in the channel plate.

2.2. Experimental procedure

The photon energy covered was 1·3 to 2·3 keV by increments of 0·5 eV. In this energy range, due to the large $2d$ spacing of KAP crystals, 26·63 Å, the Bragg angle is low (typically 15 to 20 degrees) and therefore the resolution is poor. It is typically 4 eV at 1·6 keV, so that the near-edge structures in aluminium described by Cauchois (1962), Nagakura (1964), Deslattes (1969) and Senemaud and Costa Lima (1976) are not well resolved in our experiments (figures 2 and 3(*a*)).

The intensity I transmitted through the sample and I_0 without the sample were successively recorded. At each step, five measurements were averaged so that a whole experiment needs about one and half hours. I and I_0 were then corrected for the decreasing intensity of the ACO electron beam, which is typically about 5% per hour. Figure 2 shows a photo-absorption spectrum obtained with an Al foil at room temperature. It was obtained from the experimental spectrum without any smoothing applied: the absorption background which has been subtracted was estimated in the region above the threshold by extrapolating the absorption below the edge. The photon energies have been calibrated with the inflection point of the Al K edge at 1559·3 eV (Nagakura 1964).

The EXAFS spectra shown in figures 3(*a*) and 4(*a*) were obtained by averaging three experiments. In each case, the curves were normalised by subtracting a smooth atom-like absorption obtained by drawing through the oscillations of the experimental

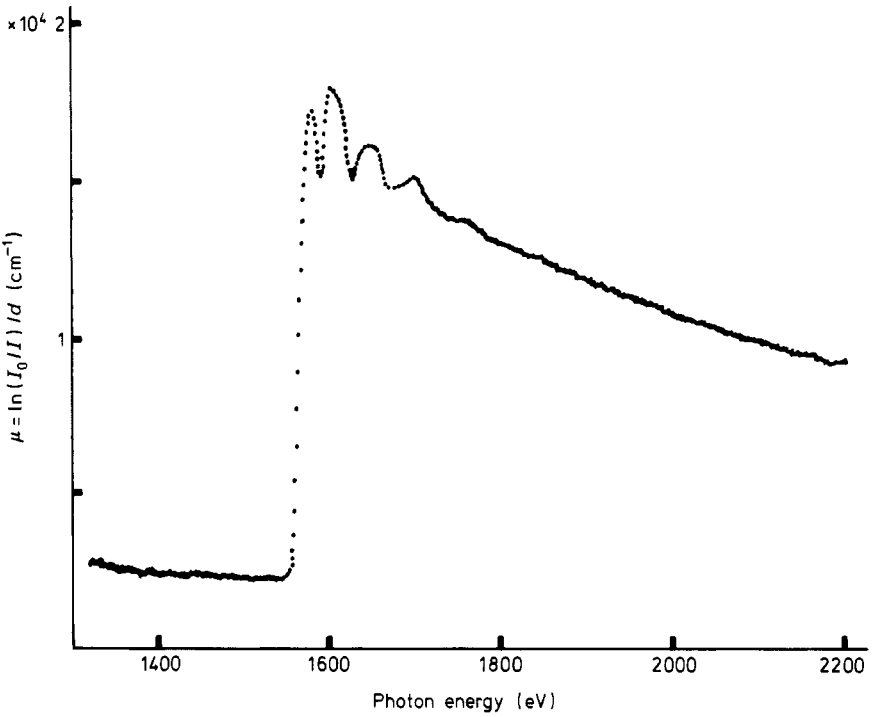

Figure 2. Absorption spectrum of a 1 μm Al sample (raw data without any smoothing). The spectrum has been measured with an ion chamber in 1·5 h with ACO operated at 540 MeV and 100 mA.

spectrum. For soft x ray experiments, samples have to be very thin because of the high atomic absorption coefficient. The metallic aluminium sample was made of two 5000 Å foils. It is, however, more difficult to have thin homogeneous films of insulators like Al_2O_3. We have prepared a suspension of alumina powder in a solution of collodion in isoamylacetate. A small drop was then deposited on a clean water surface; collodion spread then instantaneously as a thin film which still contained alumina powder. These thin films were then deposited on grids. These alumina samples were not homogeneous and the signal-to-noise ratio was thus not as good as that found with the aluminium foils.

3. First-shell EXAFS in aluminium and alumina

The EXAFS modulation factor $\chi(E)$ is determined by final state interference effects between the photoelectron wave outgoing from the ionised atom and the waves backscattered by the surrounding atoms. The backscattering factor decreases drastically with the photoelectron energy for low-Z elements. This yields a large damping of the EXAFS modulations, as shown in figures 3(*a*) and 4(*a*). It is, however, possible to analyse the data since significant signals can be obtained as far as 250 to 300 eV above the edges both for aluminium and α alumina. The edge of α alumina is shifted towards high energies with respect to the metallic aluminium edge. We find it at 1568 eV which implies a 9 eV shift. It is also broader. This is in agreement with

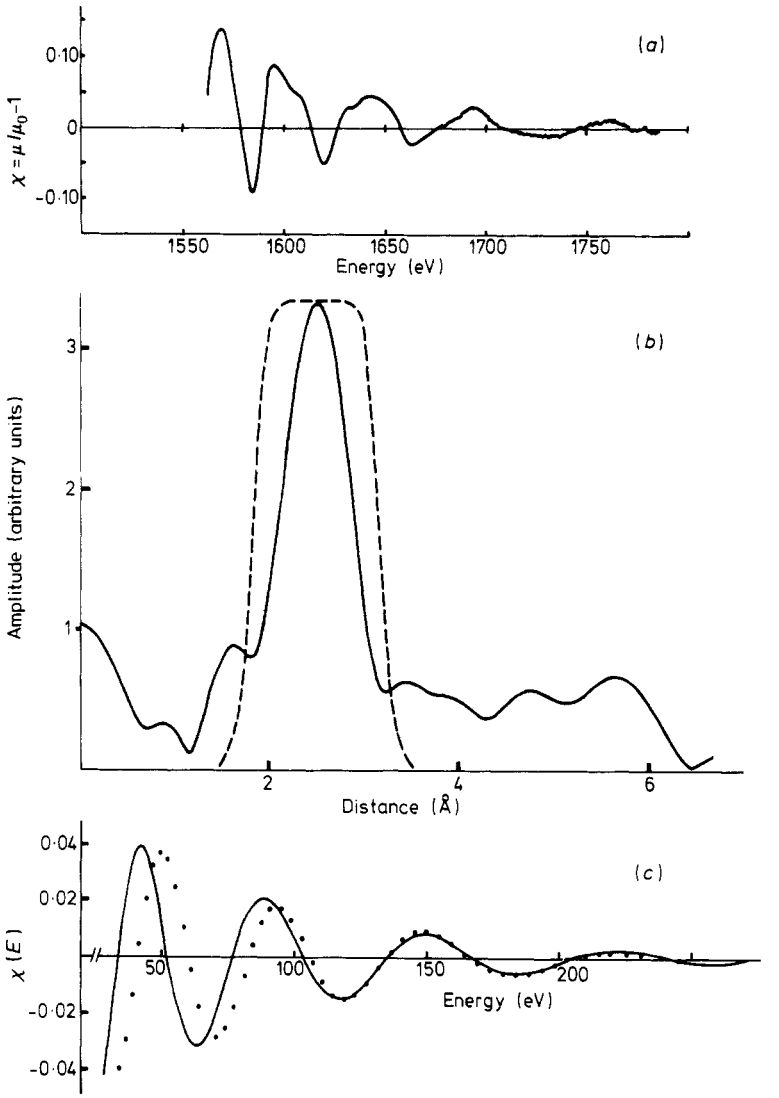

Figure 3. EXAFS of aluminium. (*a*), experimental spectrum. The zero of the energy scale corresponds to the inflection point of the edge. (*b*), absolute value of the Fourier transform of $k\,\chi(k)$. The peak at 2·45 Å corresponds to the nearest-neighbour distance 2·864 Å and is shifted by the atomic phase shifts. The broken curve is a filter window isolating the first-shell EXAFS information. (*c*), first-shell EXAFS signal back-transformed from the peak at 2·45 Å (dotted curve) and a theoretical reconstruction using atomic phase shifts and backscattering amplitudes calculated by Lee and Beni (1977) (full curve). The zero of the energy scale of the experimental curve is taken at 12 eV below the inflection point.

edge structure measurements on γ and amorphous alumina by Senemaud and Costa Lima (1976). If multiple scattering effects are neglected, the now classical theory (Ashley and Doniach 1975) gives the formula

$$\chi(k) = (-1/k)\sum_j (N_j/R_j^2)\exp(-2\sigma_j^2 k^2)\exp[-2R_j/\lambda(k)]|f_j(\pi, k)|\sin[\Phi_j(R_j, k)] \qquad (1)$$

with

$$\Phi_j(R_j, k) = 2kR_j + 2\delta_1'(k) + \arg[f(\pi, k)] = 2kR_j + \psi_j(k)$$

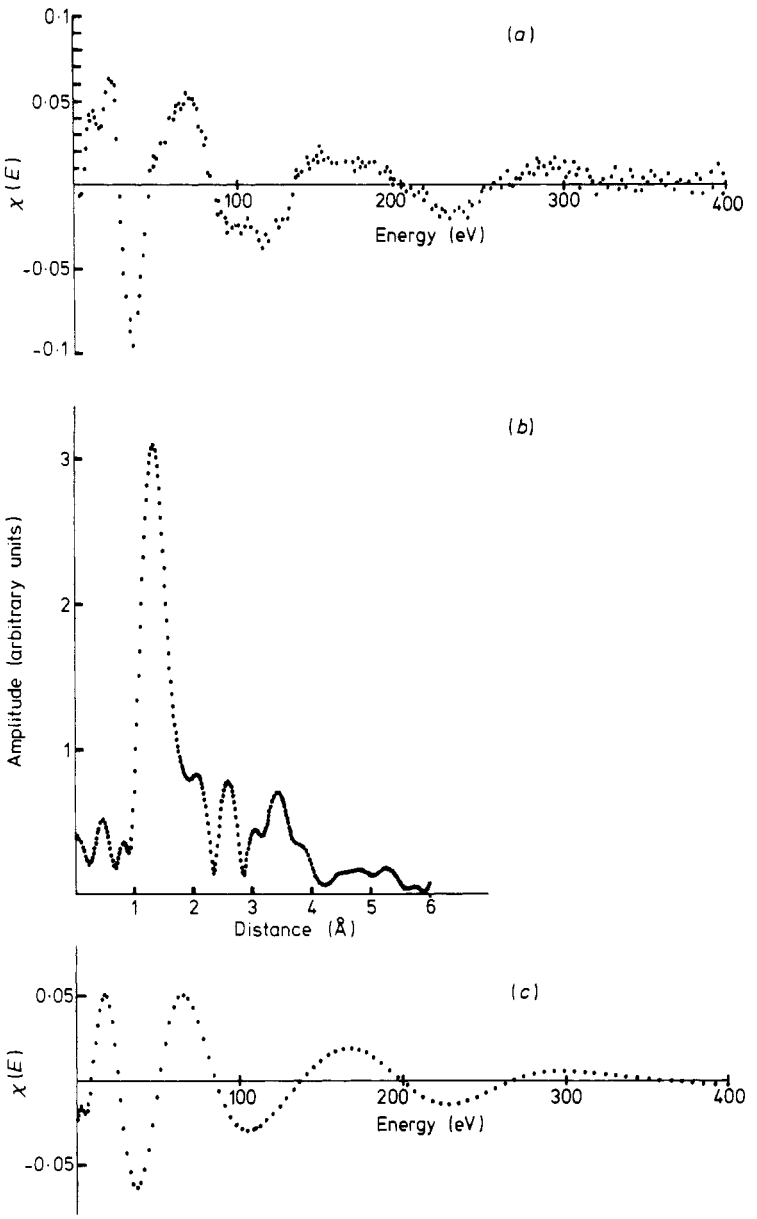

Figure 4. EXAFS of alumina. (*a*), experimental spectrum. The zero of the energy scale corresponds to the inflection point of the edge. (*b*), absolute value of the Fourier transform of $k\chi$ (k). The peak at 1·33 Å corresponds to the Al–O first-neighbour distance. (*c*), first-shell EXAFS signal back-transformed from the peak at 1·33 Å.

and

$$k = (2mE/\hbar^2)^{1/2} = [2m(\hbar\omega - E_0)/\hbar^2]^{1/2}$$

$\hbar\omega$ is the photon energy; E_0 is the so called 'threshold energy'. k is the photoelectron momentum, N_j and R_j are the number of atoms in the jth shell around the central ionised atom, and their distance to it. σ_j is the mean fluctuation of R_j and $\lambda(k)$ the electron mean free path. $f_j(\pi,k)$ is the backscattering factor of the electron wave

by the jth atom. δ'_1 is the phase shift experienced by the photoelectron in the absorbing atom. A Fourier transform of $k\chi(k)$ yields a radial distribution function whose peak is shifted by the $\psi_j(k)$ phase shift. As shown in figures 3(*b*) and 4(*b*), a prominent peak is found in both cases which is due to the first-shell contribution. A Fourier filtering can thus be performed, yielding the partial first-shell EXAFS shown in figures 3(*c*) and 4(*c*)†. The contributions of the outer shells are not resolved in the case of metallic aluminium, which is not surprising since Al has a close-packed FCC structure. In the case of alumina, they are partially resolved; however, their analysis is difficult since Al–Al and Al–O distances contribute to the same peaks (Wyckoff 1964). It is clear from equation (1) that the nearest-neighbour distance can be extracted from the partial first shell EXAFS provided the atomic phase shifts $\delta'_1(k)$ and arg $(f_j(\pi,k))$ are known and the E_0 threshold energy is correctly determined. E_0 would be the energy level at the bottom of the conduction band in a free-electron gas model. For a real bandstructure, E_0 is not so easy to determine and would be better taken as an adjustable parameter within a few eV of the experimental threshold (Lee and Beni 1977). However, an adjustment of E_0 results in a change in the phase shifts which decreases with the electron momentum as $1/k$. A coherent procedure has to be used in order to get a correct determination of the R_j values (Martens *et al* 1978). For a given set of phase shifts, and some arbitrary value of E_0, we get a set of k-dependent $R(k,E_0)$ values from the locations of the zeros of the partial EXAFS which are given by

$$2kR_1 + \psi_1(k) = m\Pi. \tag{2}$$

The atomic phase shifts $\psi_1(k)$ are calculated modulo 2Π; however, a rough knowledge of R_1 gives an unambiguous determination of m, since changing m by 1 shifts the R value by 0·8 Å at 200 eV and 0·4 Å at 700 eV. The E_0 energy is then adjusted until one gets a set of $R_1(k,E_0)$ values which do not depend on k. Such a procedure gives an accurate determination of R_1; the standard deviation of the $R(k)$ values may be lower than 6×10^{-3} Å when a significant EXAFS signal extends over 500 eV (Fontaine *et al* 1979).

This procedure has been used both for aluminium and α alumina spectra. The atomic phase shifts were taken from Lee and Beni (1977).

In the case of aluminium, we get $R(k)$ curves which are flat at high photoelectron energies ($E > 150$ eV) when the zero of the energies is taken at 12 eV below the inflection point, as shown in figure 5. In this range, the mean value is 2·87 Å, which is very close to the 2.864 Å well known first-neighbour distance (Wyckoff 1964). As is also shown in figure 5, the accuracy in the determination of E_0 is better than 2 eV, yielding an accuracy in the distance measurement of 0·01 Å. However, at energies lower than 150 eV there is a systematic decrease of the determined distance with the photoelectron energy, which may result in errors up to 0·1 Å at 50 eV from the edge. This will be discussed in the next section. Finally we should like to make two comments. First, we find that the zero of the photoelectron energy is at the bottom of the conduction band, which in aluminium is at 11·7 eV below the Fermi level, i.e. the inflection point of the absorption spectrum. This is very pleasant since the zero of energy in Lee and Beni's phase shifts has to be taken as the zero of the muffin tin, which in aluminium is close to the bottom of the conduction band.

† Several windows have been checked that did not affect much the locations of the zeros of the partial EXAFS signal. Their displacements were smaller than 2·5 eV, even in the high-energy part of the spectrum $E > 200$ eV.

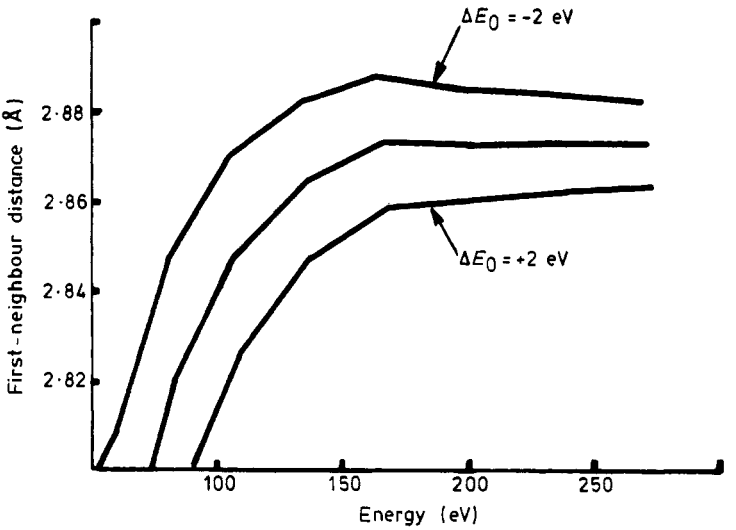

Figure 5. The first-neighbour distance in aluminium is determined from the locations of the zeros of the curve shown in figure 3 (*c*) and plotted against the energy of the photoelectron. The E_0 zero of the energy scale is taken at 12 eV below the inflection point of the edge. Three curves are shown for E_0 respectively equal to 0, +2 and −2 eV.

We think that such an agreement is not casual, but is due to the very simple electronic structure of aluminium, which is a good example of a free-electron-like metal.

The second point concerns the amplitude of the partial EXAFS signal. As is shown in figure 3(*c*), it can be fitted correctly using the backscattering amplitudes calculated by Lee and Beni (1977) and formula (1) with $\phi = 0{\cdot}14$ Å and $\lambda = 1{\cdot}3\,k$ (λ in Å and k in Å^{-1}). The linear dependence of the electron mean path is of course a rough approximation: it nevertheless yields values which are in the expected range of magnitude, for example 4 Å at 50 eV. Finally, we also point out that the dip found at 25 eV above the absorption edge in the EXAFS spectrum shown in figure 3(*a*), which has been attributed by Senemaud and Costa Lima (1976) to the presence of localised d states in the density of empty states, appears to be one of the negative EXAFS oscillations.

Figure 6 shows the $R(k)$ determinations for α alumina and for the best choice of E_0, which turns out to be 11 eV below the inflection point. The dispersion of

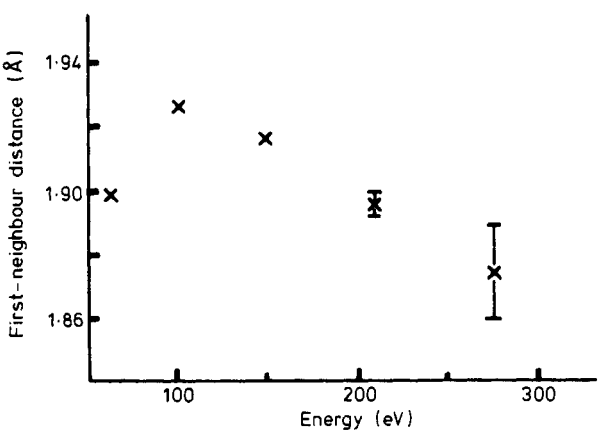

Figure 6. First-neighbour Al–O distance in α alumina. Same determination as in figure 5. E_0 is taken at 11 eV below the inflection point.

the $R(k)$ determinations is larger than that found for aluminium, due to the poorer quality of the EXAFS spectrum. However, the average distance which is thus determined is 1·904 Å. It compares well with the average Al–O nearest-neighbour distance of 1·915 Å in α alumina, where each Al atom is surrounded by three Al atoms at 1·86 Å and three at 1·97 Å (Wyckoff 1964).

It has been impossible to separate these two inequivalent distances. Our Al-K-edge analysis of the EXAFS in bulk alumina is in good agreement with the surface EXAFS analysis of an oxidised Al surface recently performed by Stöhr *et al* (1978*b*) on the OK edge. They find a mean O–Al distance of 1·92 Å, so that experiments on both Al and OK edges yield the correct distance within 0·01 A.

4. Screening effect in metallic aluminium

As shown in figure 3(*c*), the theoretical reconstruction of the first-shell EXAFS in Al using Lee and Beni's phase shifts (Lee and Beni 1977) fits the experimental result well for energies higher than about 130 eV above the edge. However, in the range 50 to 130 eV there is a systematic disagreement which decreases when increasing the photoelectron energy. Such a systematic effect has not been found with germanium and copper, which Lee and Beni analysed very carefully. This is rather surprising, since Al is a free-electron-like metal for which the EXAFS theory is better suited than for Cu or Ge.

A more direct comparison is shown in figure 7. Using the well known nearest-neighbour distance in Al (2·864 Å) we have determined the atomic phase shift $\psi(k)$ from the locations of the zeros of the EXAFS signal. A comparison with Lee and Beni's calculations for $\psi(k) = 2\ \delta_1'(k) + \arg f(\pi,k)$ shows that the calculated values are too large for low photoelectron kinetic energies. At these energies, the electron scattering should be treated using a spherical expansion which takes into account

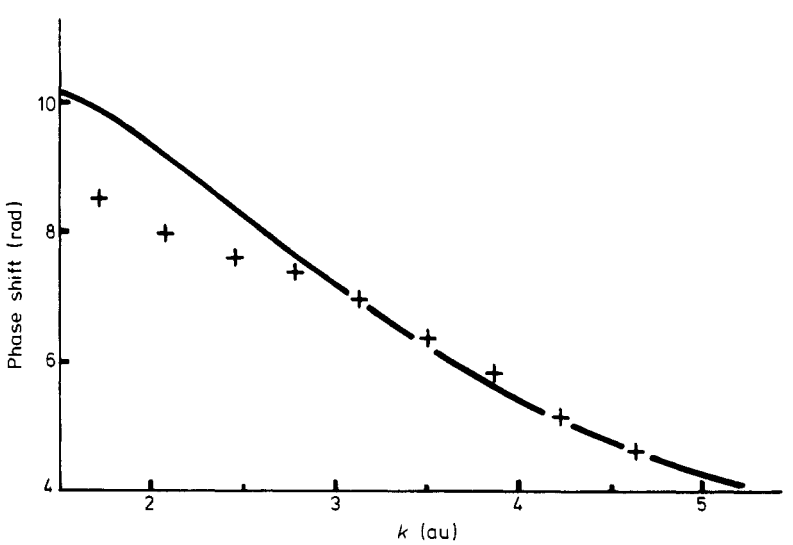

Figure 7. Comparison between the experimentally determined phase shift Ψ (+) for Al–Al bonds in aluminium and the theoretical values calculated by Lee and Beni (1977) (full curve). The zero of the energy scale for the experimental results is taken at 12 eV below the inflection point.

the finite size of the atoms. This has been shown to increase the backscattering phase shift by about 1 rad at 50 eV and 0·4 rad at 150 eV in the case of copper (Lee and Pendry 1975). Since the aluminium atom is about the same size as the copper atom, the effect is likely to be quantitatively similar in the case of Al, so that the discrepancy between experimental and theoretical phase shifts would be even larger below $k = 3$ au if the spherical wave expansion was used. In the case of Al_2O_3, however, the use of the spherical wave expansion would improve the analysis of the experimental results, since an increase of the phase shift when decreasing the energy below 150 eV would lower the $R(k)$ determinations in this energy range, thus yielding a more flat $R(k)$ curve than the one shown in figure 6.

Alumina is an insulator, while Al is a free-electron-like metal. Thus a simple explanation of the different behaviour of the phase shifts in Al and Al_2O_3 may be related to the screening of the K hole in Al by the conduction electrons. This would reduce the potential experienced by the photoelectron inside the central atom in the case of elemental aluminium. It has often been argued that such an effect should be important only at very low photoelectron energies comparable to the plasmon energy. This point has been recently discussed by Noguera *et al* (1979). They show that the screening of a deep hole by conduction electrons in a metal does occur after a critical time t_0, which is typically 0·15 times the plasmon period, t_0 being the time necessary for the creation of the plasmon. The photoelectron will thus see a statically screened potential in the central atom if the characteristic time t_0 is smaller than the time d/v, where d is the distance between the photoexcited atom and the backscattering atom and v is the speed of the photoelectron. For aluminium, where the plasmon energy is 15·3 eV (Raether 1965, Daniels *et al* 1970) we thus have a characteristic photoelectron momentum $k_c \sim 3$ au, which is in agreement with the results shown in figure 7.

A preliminary calculation by C Noguera (private communication) yields a quantitatively correct magnitude for the lowering of the $2\delta_1'$ central atom phase shift when the dynamic screening of the K hole in elemental Al is calculated within the semiclassical model developed by Noguera *et al* (1979), and within the muffin-tin approximation. We thus would like to point out here that the screening of the K hole by the conduction electrons may have important effects on the phase shifts experienced by the photoelectron in metals having well defined high-energy plasmons, at least for low photoelectron energies $E < 150$ eV. From that point of view, Al appears to be a good candidate. In copper ($\omega_p \sim 7{\cdot}2$ eV), the effect should thus be important only at a very low electron momentum $k \sim 1{\cdot}5$ au, where the EXAFS theory is no longer correct. Therefore it is not surprising that the fits performed for copper by Lee and Beni (1977) with an unscreened atom are very good, even at 50 eV from the edge.

5. Conclusions

EXAFS experiments are now feasible in the soft x-ray range 600 eV to 2·5 keV using a rather conventional technique; we just use a Bragg spectrometer and measure the photoabsorption through the sample. EXAFS can thus be measured on the K edges of the light elements like Si or Mg which have technical or biological interest. We have given here a first example of an EXAFS measurement on the Al K edge in aluminium and α alumina, and shown that accurate determinations of the

nearest-neighbour distances are possible even for low-Z elements where the K edge EXAFS is restricted to a 200 or 300 eV range.

In the case of aluminium, which is a free-electron-like metal with well defined high-energy plasmons, we have also emphasised the importance of the screening effect in metals, which may drastically change the atomic phase shift within 150 eV from the edge. This effect may be important for surface EXAFS analysis where the signal is often limited to a low-energy range.

Acknowledgments

We thank Professor J Friedel for his interest and comments, and C Noguera and D Spanjaard for many discussions on the screening effect on phase shifts. We also acknowledge the valuable technical help of M Lemonnier, C Depautex and the LURE staff.

References

Ashley C A and Doniach S 1975 *Phys. Rev.* B**11** 1279
Bianconi A and Bachrach R Z 1979 *Phys. Rev. Lett.* **42** 104
Brown F C, Bachrach R Z and Lien N 1978 *Nucl. Instrum. Meth.* **152** 73
Cauchois Y 1962 *Acta Crystallogr.* **5** 351
Daniels J, Festenberg C, Raether H and Zeppenfeld K 1970 *Springer Tracts Mod. Phys.* **54** 77
Deslattes R D 1969 *Acta Crystallogr.* A**25** 89
Fontaine A, Lagarde P, Naudon A, Raoux D and Spanjaard D 1979 *Phil. Mag.* to be published
Lee P A and Beni G 1977 *Phys. Rev.* B**15** 2862
Lee P A and Pendry J B 1975 *Phys. Rev.* B**11** 2795
Lemonnier M, Collet O, Depautex C, Esteva J M and Raoux D 1978 *Nucl. Instrum. Meth.* **152** 109
Martens G, Rabe P, Schwentner N and Werner A 1978 *Phys. Rev.* B**17** 1481
Nagakura I 1964 *Sci. Rep. Tohoku University* **48** 37
Noguera C, Spanjaard D and Friedel J 1979 *J. Phys. F: Metal Phys.* **9** 1189
Raether H 1965 *Springer Tracts Mod. Phys.* **38** 84
Sayers D, Stern E and Lytle F 1970 *Adv. X-Ray Analysis* **13** 248
Senemaud C and Costa Lima M T 1976 *J. Phys. Chem. Solids* **37** 83
Stöhr J 1979 *J. Vac. Sci. Technol.* **16** 37
Stöhr J, Denley D and Perfetti P 1978a *Phys. Rev.* B**18** 4132
——1978b *SSRL Report* 78-06, Stanford University
Wyckoff R W G 1964 *Crystal Structures* (New York: Wiley)